Clays and Clay Minerals, Vol. 45, No. 1, 99–109, 1997.

SMECTITE ILLITIZATION IN PLIOCENE-AGE GULF OF MEXICO MUDROCKS

J. H. RASK,[1] L. T. BRYNDZIA,[2] N. R. BRAUNSDORF[3] AND T. E. MURRAY[4]

[1] Shell Western E&P Company, 200 N. Dairy Ashford, Houston, Texas 77079

[2] U.S. EPA/NRMRL, 5995 Center Hill Drive, Cincinnati, Ohio 45224

[3] Shell E&P Technology Company, Bellaire Technology Center, PO Box 481, Houston, Texas 77001

[4] Shell Development Company, Westhollow Technology Center, PO Box 1382, Houston, Texas 77001

Abstract—Utilizing high-resolution transmission electron microscopy (TEM), energy-dispersive spectroscopy (EDS) and X-ray diffraction (XRD) techniques, we have studied the transition from shallower smectite-rich mudrocks to deeper illite-rich mudrocks in Pliocene-age turbidite sediments from the northern Gulf of Mexico (GOM). Our objective in this work was to better understand how the smectite-illite transition may affect the onset of geopressuring in GOM sediments. The samples studied were sidewall cores from an offshore Louisiana well. In previous studies of GOM sediments, the smectite-to-illite reaction has mainly been documented in considerably older, Miocene-age sediments.

The results of this study elucidate the reaction mechanisms entailed in the transformation of clays in this sediment from smectitic to illitic. We found that illite formed at the expense of smectite in 2 ways: 1) growth of preexisting discrete illite flakes, and 2) creation of new illite layers within mixed-layer illite-smectite. Also, illitization apparently proceeded via a dissolution/precipitation, Al-conserving reaction rather than a solid-state, layer-conserving reaction. Smectite illitization is commonly believed to require input of K from feldspar dissolution. Our XRD results found little correlation between decreases in K-feldspar and increases of illite. However, in 1 instance TEM/EDS analyses indicated the presence of high-charge smectite, which suggests that insufficient K was available for illitization. TEM images also show small packets of authigenic chlorite in illite-rich mudrock. This chlorite may act as a sink for Fe liberated upon smectite illitization.

Key Words—Clay Diagenesis, Core Analysis, Gulf of Mexico, Illite, Smectite, TEM, XRD.

INTRODUCTION

The transformation of smectite to illite has been recognized as an important reaction in the diagenesis of clay minerals in clastic marine sediments from many basins worldwide (Burst 1969; Pearson et al. 1982; Velde and Vasseur 1992). In GOM sediments, this reaction has been documented in Miocene-age and older rocks (Burst 1969). Analyses of newly deposited, unaltered GOM sediment have found that its clay component is mostly interstratified illite/smectite, with smectite predominating (Burst 1969; Hower 1981). With increasing temperature (i.e., depth of burial), smectite in sediments is transformed to illite (Perry and Hower 1970; Surdam and Crossey 1987). Studies of GOM sediments indicate that this reaction ceases once the proportion of expandable layers (smectite) in mixed-layer clay reaches ~20% (Hower et al. 1976; Bell 1986; Eberl 1993).

Dramatic reductions have been noted in the smectite-to-illite ratio at depths corresponding to temperatures near 100 °C (Perry and Hower 1970). However, significant variability in this reaction temperature has been reported (Freed and Peacor 1989a). The work of Velde and Vasseur (1992) suggests that the extent of illitization is dependent on both time and temperature.

The compositional differences between smectite and illite are also important to smectite illitization. Because of these differences, it has been proposed that the smectite-to-illite reaction requires input of K and Al, and results in the generation of Si, Fe and water. The following reaction outlines mineralogical changes commonly thought to be associated with the smectite-to-illite reaction (Hower et al. 1976):

$$\text{K-feldspar} + \text{Smectite} \rightarrow \text{Illite} + \text{Chlorite} + \text{Quartz} \quad [1]$$

In this model reaction, K-feldspar dissolution provides K and Al needed for illitization. The Si freed by the reaction precipitates as quartz cement, and authigenic chlorite is postulated as the sink for liberated Fe.

A variation in this illitization reaction that entails a net loss of clay and requires no Al input was proposed by Boles and Franks (1979). They noted evidence for this reaction in the XRD results of Hower et al. (1976), in which the total of illite plus smectite decreases as illitization proceeds. Other evidence for this Al-conserving reaction is provided by microprobe determinations of clay compositions in shales from the Frio formation (Shaw and Primmer 1989). These analyses found that deeper, illitic, mixed-layer clays actually contained slightly less Al than shallower, more smectitic mixed-layer clays.

TEM and its associated techniques of electron diffraction and EDS have proven to be valuable tools for

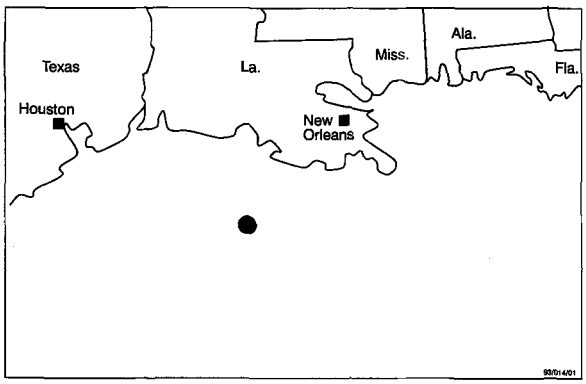

Figure 1. Map showing the location of the study well.

studying the transition of smectite to illite. TEM studies of clays typically concentrate on imaging clay interlayer spacings. Although hydrated smectite has a larger interlayer spacing than illite, in the vacuum of the TEM the interlayer spacing of smectite collapses to about 10 Å, the same spacing as illite (Klimentides and MacKinnon 1986). To distinguish smectite from illite in TEM images, microscopists have used morphology differences (Ahn and Peacor 1986), special imaging conditions (Guthrie and Veblen 1989; Veblen et al. 1990), special intercalating molecules (Vali and Koster 1986) and ultra-high-resolution TEM imaging (Ahn and Buseck 1990).

TEM images of smectite-rich mudrocks typically show a matrix of curled smectite-rich mixed-layer clay with scattered thin linear packets of ordered illite layers. In images of more illitized samples, illite packets are more prevalent and larger (Ahn and Peacor 1986). Also, high-resolution images of illitized samples show illite interlayered with smectite (Ahn and Buseck 1990), as expected according to the mixed-layer clay model.

Our study of this reaction was primarily motivated by the correlation that has been noted in Gulf Coast sediments between the smectite-to-illite reaction and the onset of geopressures (Freed and Peacor, 1989b). In this work, we analyzed mudrock samples from a GOM continental shelf well in which the onset of geopressures coincides approximately with the depth of the smectite-to-illite reaction. Our goal was to learn more about the mechanisms of this reaction to better explain its relationship to geopressuring.

SAMPLES AND ANALYTICAL TECHNIQUES

Sidewall core samples were taken from a GOM continental shelf well located approximately 185 km (115 mi) south of the central Louisiana coast (Figure 1). In this project, a total of 75 mudrock samples from this well were examined. These samples span the depth interval from 2882 to 4159 m (9454 to 13,645 ft) below sea level. Across this interval, well-logs show evidence of geopressuring by gradual decreases in mudrock density, velocity and resistivity (Figure 2). Temperatures in this depth interval range from ~80 to 107 °C (176 to 225 °F), which is the temperature range typically associated with the smectite-to-illite reaction (Perry and Hower 1970). The corrected static bottom hole temperature at 4175 m (13,699 ft) is 107 °C, corresponding to a thermal gradient in this well of ~20 °C/km (0.011 °F/ft).

XRD was used to determine phase compositions of the bulk and the clay fraction (< 4 μm) for 53 samples. For 22 additional samples, XRD analyses were run for only the clay fraction. To collect XRD data, we used a Scintag θ-θ diffractometer with a solid-state Ge detector and sample spinner. The scan rate used was 2°/min. The methods described by Moore and Reynolds (1989) were used to determine the bulk percentages of clay minerals and the smectite-to-illite ratio of the mixed-layer clays. Representative XRD scans of a smectite-rich and an illite-rich sample are illustrated in Figure 3.

Three samples, from depths of 2899, 3829 and 4127 m (9511, 12,563 and 13,541 ft), were selected for TEM characterization, which included compositional analysis by EDS. Specially prepared petrographic thin sections were used to make ion-thinned samples for TEM. The thin sections were cut perpendicular to clay layering and bedding to facilitate study of interlayer textures. TEM slot grids were glued to selected areas of the thin sections, the underlying epoxy was melted and the fragile mudrock slices were carefully removed from the thin sections. A Gatan Model 600A Dual Ion Mill was used to thin the ~30-μm slices of mudrock to the ~0.1-μm thickness required for TEM. Samples were monitored periodically during ion-milling by imaging in an environmental scanning electron microscope.

The ion-milled mudrock samples were studied using a 300-KeV Philips 430 TEM with an accessory video camera. Sample grids were held in place within the TEM by a double-tilt, side-entry sample holder. Because of the sensitivity of smectite and illite to the electron beam, we attempted to minimize beam exposure on areas of clay. The video camera allowed focusing and astigmatism correction of images with minimal beam damage. Elemental analyses of selected areas of samples observed in the TEM were obtained using an EDAX EDS detector in conjunction with a Noran multi-channel analyzer.

Illite is distinguished from smectite in TEM images on the basis of crystallite morphology (Freed and Peacor 1989a, 1989b). Smectite is recognized by its characteristic curling texture and subparallel 10-Å lattice fringes, which often appear disordered (Figure 4a). Discrete illite is texturally distinct, occurring as packets several layers wide with ordered, parallel 10-Å lattice fringes (Figures 4b and 4c). Illite within mixed-

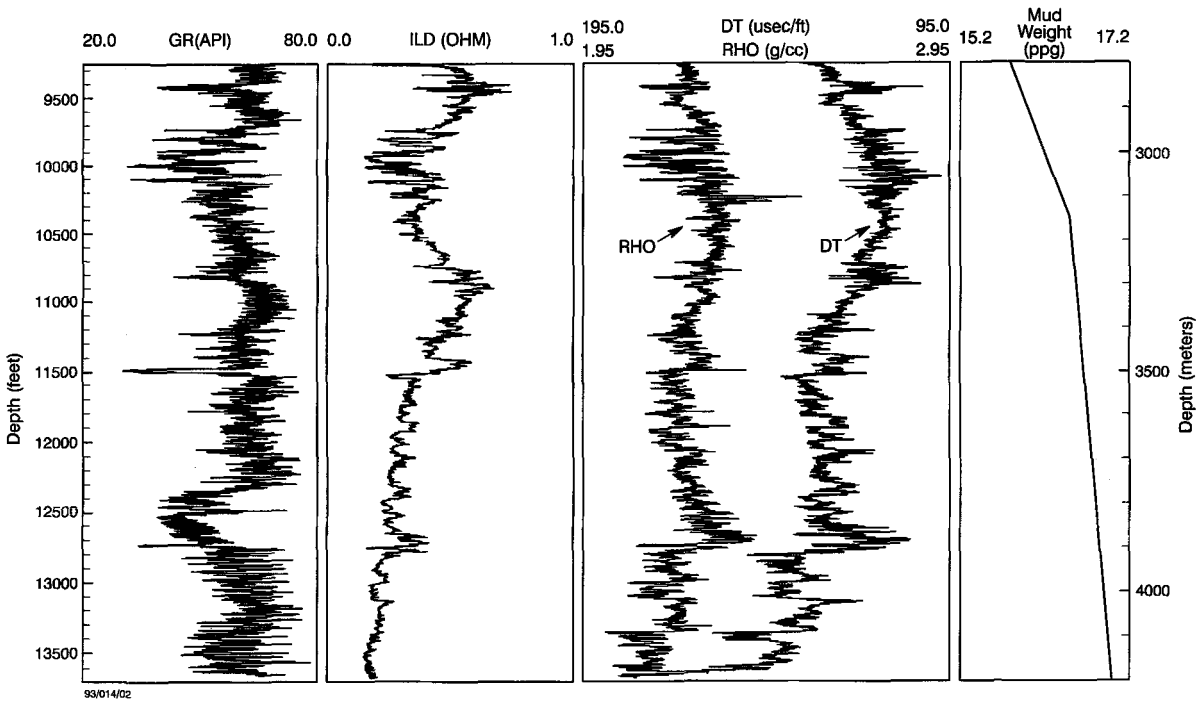

Figure 2. Wireline log suite and drilling mud weights from the study well. Note the gradually decreasing density (RHO), velocity (DT) and resistivity (ILD), and the increasing mud weight (MW) in the interval below 3200 m (~10,500 ft). These data are consistent with an increase in fluid pressure occurring in the interval in which our XRD and TEM analyses detect illitization of smectite.

layer clay is difficult to identify, particularly in smectite-rich mixed-layer material. Illite-rich mixed-layer clay is typified by textures in which very thin packets of parallel illite layers are seen in a subparallel arrangement (Figure 4c).

Cation percentages for nanometer-sized areas of clays observed in the TEM were derived from EDS spectra. Under optimum conditions, EDS in the TEM can be used to determine elemental compositions of areas as small as 100 Å with analytical uncertainty of ~5% (MacKinnon 1990). Software provided with the Noran multichannel analyzer (the Standardless Metallographic Thin Film program) was used to perform ZAF corrections, then calculate elemental percentages. Calibration factors provided by the software were used in calculations of elemental percentages, after they had been checked by analyses of standard samples. Work with kaolinite and K-feldspar standards indicates that our EDS-derived values for Al and Si are accurate to within ~5%. The analytical uncertainty is significantly greater for other elements that are present at lower concentrations. Values for light elements such as Na are especially suspect. Na gives low-energy X-ray signals, and the background beneath its EDS peak is difficult to model. In addition, the electron beam causes diffusive loss of Na away from the area exposed to the beam. Therefore, our assessments of cation percentages for elements other than the major cations Al and Si should be considered rough estimates of the actual concentrations.

To derive mineral formulae, cation proportions were fit to the following stoichiometric form for dioctahedral illite/smectite clays:

$$Na_{X1}K_{X2}Ca_{X3}(Al_{Y1}Fe_{Y2}Mg_{Y3})(Si_{Z1}Al_{Z2})O_{10}(OH)_2{\cdot}nH_2O \quad [2]$$

Some assumptions were made to convert cation proportions from EDS into numbers that match this stoichiometry. First, the amount of each cation per formula unit was calculated, assuming that the cation charge per formula unit equals 22. Aluminum was then apportioned between the tetrahedral and octahedral sites assuming that Si plus Al in the tetrahedral site equals 4.0. The remaining Al was assigned to the octahedral site, along with all Fe and Mg. All K and Ca were assigned to interlayer sites. As mentioned previously, Na concentrations appeared to be very low, but our analyses of this element were unreliable. For this reason, Na was omitted from our approximated formulae. Clay mineral stoichiometries derived from selected EDS analyses are given in Table 1. These analyses may sample exclusively illite/smectite clay because the areas analyzed are very small, typically 10's of nm in diameter.

https://doi.org/10.1346/CCMN.1997.0450112 Published online by Cambridge University Press

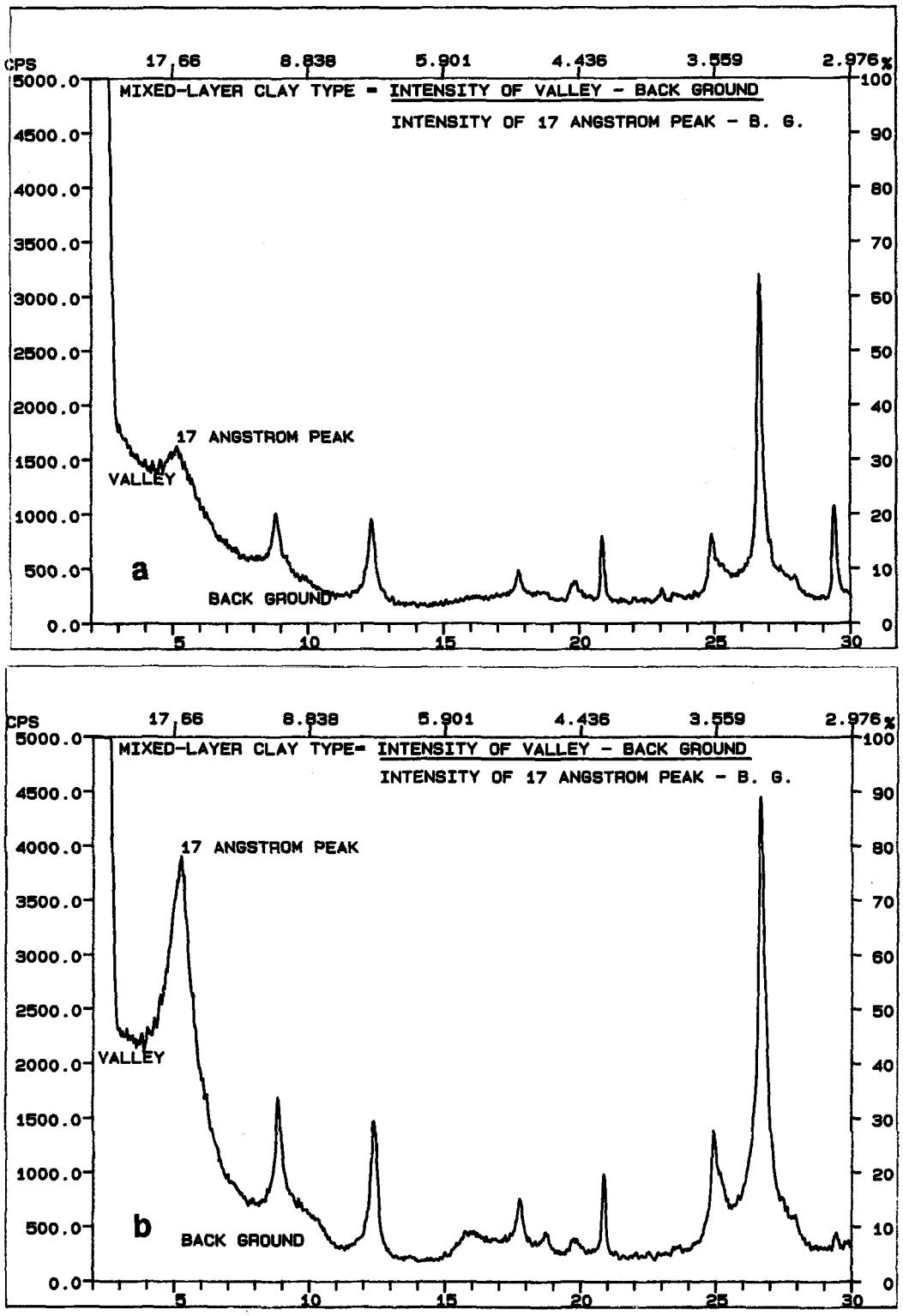

Figure 3. XRD traces illustrating the characteristic peaks that were used to distinguish and quantify smectite and illite in this work. a) A typical pattern from a smectite-rich sample. b) A typical pattern from an illite-rich sample.

https://doi.org/10.1346/CCMN.1997.0450112 Published online by Cambridge University Press

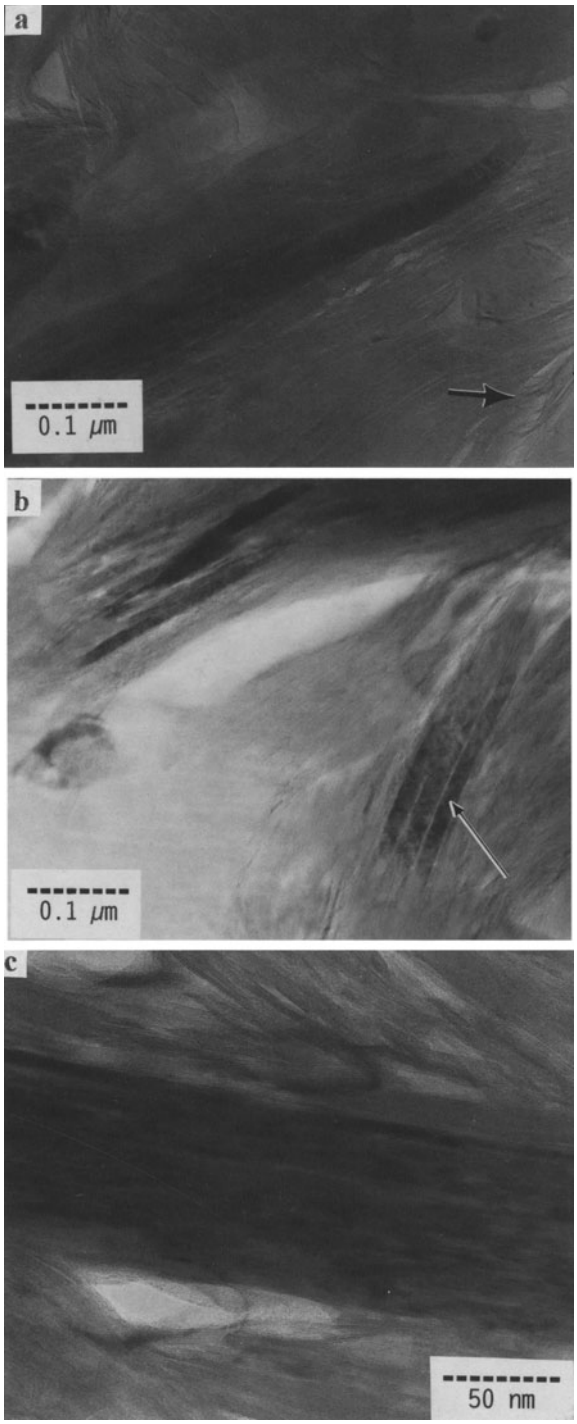

Figure 4. TEM images of mudrock samples. a) TEM image of sample from 2899 m. Curling layers of smectite are evident in the area marked by the arrow. Composition of clay in this sample is given by stoichiometry #1 in Table 1. b) TEM image of sample from 3829 m. The narrow, dark ribbons in this image are packets of illite viewed in cross section. Fine parallel 10-Å illite layers are visible within the packets. Composition of clay in the area indicated by the arrow is given by stoichiometry #2 in Table 1. c) TEM image of sample from 4127 m. The central dark ribbon is a packet of discrete illite. Surrounding this packet is illitic mixed-layer clay.

RESULTS of XRD and TEM ANALYSIS

Mineralogy and Clay Composition

XRD analyses of the clay fraction of mudrock samples from the study well show a marked decrease in smectite with depth and a corresponding increase in total illite Figures 5a and 5b). The greatest change in the composition of the clay occurs between approximately 3350 and 3650 m (~11,000 to 12,000 ft, which corresponds to the temperature range 90 to 96 °C. Paleontological examination of foraminifera and nannoplankton indicates a Pliocene age for the samples in the reaction interval (*Valvulineria "H"* to *Globigerina nepenthes*); the Pliocene/Miocene boundary in this well is approximately at depth 13,300 ft. The total depth range of the samples (9454 to 13,645 ft) spans the age range represented by the following faunal picks: Foraminiferal range, *Globorotalia miocenica* to *Buliminella 1*; Nannoplankton range, *Discoaster pentaradiatus* to *Sphenolithus verensis.* The age, thermal gradient (20 °C/km) and clay composition in the study well are comparable to those for recent sediments in the Los Angeles Basin, California, where the illitization of smectite has been documented by Velde and Vasseur (1992). We believe that this is the first documented example of smectite illitization in GOM Pliocene-age sediments.

In the shallowest sample examined by TEM, from 2899 m (~80 °C), XRD results indicate that the clay fraction is 48% mixed-layer clay (85% smectite and 15% illite), and 40% discrete illite. TEM images are consistent with this mineralogy, showing predominantly curling smectite, with isolated discrete packets of illite (Figure 4a). An EDS analysis of clay in this area gives stoichiometry #1 in Table 1. The stoichiometry is consistent with the interpretation that the analyzed area is a mixed-layer clay with illite and smectite.

In the next-deepest sample examined by TEM, from 3829 m (~100 °C), the clay fraction consists of 46% discrete illite and 41% mixed-layer clay, with the mixed-layer material comprising 60% smectite. TEM images show that illite packets are more prevalent than in the shallower sample, which reflects increased illitization with depth (Figure 4b). EDS analyses of this middle sample are given as stoichiometries #2 and #3 in Table 1, and indicate that significant variability exists in its clay compositions. An EDS spectrum from the area indicated by the arrow in Figure 4b, within individual illite packets, yields an estimated Al/Si ratio close to that of illite. As expected, the clay in this sample that appears more smectitic produces an EDS spectrum with lower estimated Al/Si ratios (#3 in Table 1).

An even higher degree of illitization is evident in images of the deepest sample studied by TEM, from 4127 m (~106 °C, Figures 4c and 6). XRD analysis

https://doi.org/10.1346/CCMN.1997.0450112 Published online by Cambridge University Press

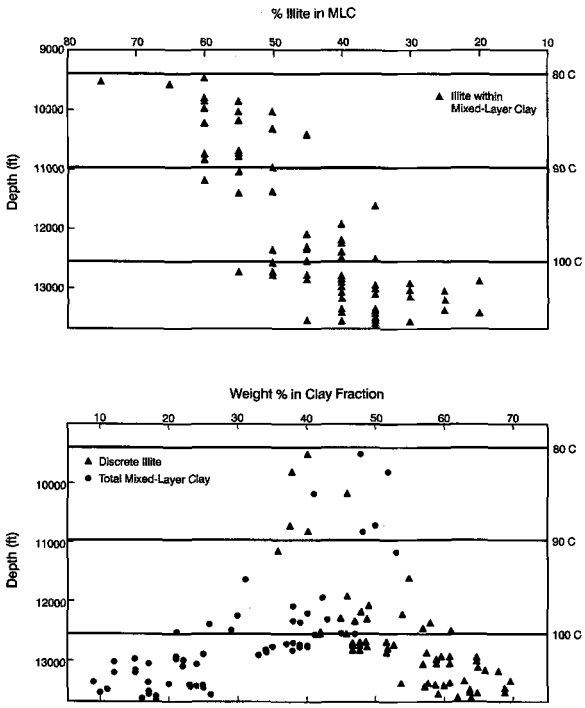

Figure 5. Plots of depth vs. XRD data from 75 mudrock samples of the study well. a) Increase of illite within mixed-layer clay with increasing depth and temperature. b) Increases of discrete illite and decreases of mixed-layer clay in the clay fraction with increasing depth.

indicates that the clay fraction in this sample consists of 69% discrete illite and only 10% mixed-layer clay. The mixed-layer clay is 45% smectite and 55% illite. In TEM images, large, discrete packets of illite are abundant. Mixed-layer clay contains smaller groups of parallel layers that we interpret to be illitic. Discrete illite and illite within mixed-layer clay are both seen in Figure 4c. The ~800-Å-thick illite packet that traverses this image is a representative example of discrete illite. Growth of such large packets of illite accounts for the increase in discrete illite detected by XRD. The thin, needle-like crystallites consisting of 3 to 10 parallel layers seen above and below the large packet are interpreted to be illitic mixed-layer clay. Illitization of mixed-layer clay is likely reflected in TEM images by increased numbers of such thin crystallites.

Table 2. XRD data from 5 mudrock samples from the study well, including the 3 samples selected for TEM study. The listed numbers reflect the wt% of the phases in the samples, as determined by the BRC XRD lab. For each sample, 2 XRD analyses were run, 1 of the bulk sample and 1 of the separated clay fraction (particles 0.26 to 4.7 μm).

Sample depth m (ft)	2899 (9511)	3404 (11,168)	3829 (12,563)	4075 (13,368)	4127 (13,541)
Bulk fraction					
Mixed-layer clay	13	20	29	10	17
PCT smectite in MLC	85	70	60	50	45
Illite	19	14	26	30	33
Kaolinite	4	2	5	9	6
Chlorite	2	1	1	1	1
Calcite	0	0	2	5	2
Dolomite	6	1	2	5	5
Siderite	1	2	2	1	3
Albite	6	5	3	4	4
K-feldspar	5	5	3	3	3
Quartz	44	38	24	31	26
Clay fraction					
Mixed-layer clay	48	53	41	9	10
PCT smectite in MLC	85	70	60	50	45
Illite	40	36	46	70	69
Kaolinite	11	9	11	18	19
Chlorite	2	1	1	2	3

Clay Mineral Textures

XRD analyses identified smectite only as a component of mixed-layer I/S, while 2 types of illite are distinguished: 1) illite as a component of mixed-layer I/S, and 2) separate, discrete illite. XRD results show that, with increasing depth, mixed-layer clay becomes more illitic, the total mixed-layer clay component decreases and discrete illite becomes more abundant (Table 2; Figures 5a and 5b). TEM images, consistent with the XRD results, indicate that both the number and the size of discrete illite packets increase with increasing illitization. Our XRD and TEM results indicate that increases in discrete illite result from both growth onto detrital illite packets, and nucleation and growth of authigenic illite packets within the mixed-layer clay. The XRD-defined component of discrete

Table 1. Clay mineral stoichiometries from EDS analyses of mudrocks.

Sample depth m (ft)		Stoichiometry of clay minerals
2899 (9511)	1	$K_{0.22}(Al_{1.4}Fe_{0.47}Mg_{0.11})(Si_{38}Al_{0.2})O_{10}(OH)_2{\cdot}nH_2O$
3829 (12,563)	2	$K_{0.26}(Al_{1.4}Fe_{0.45}Mg_{0.41})(Si_{3.6}Al_{0.4})O_{10}(OH)_2{\cdot}nH_2O$
	3	$K_{0.15}Ca_{0.03}(Al_{1.4}Fe_{0.28}Mg_{0.27})(Si_{4.1})O_{10}(OH)_2{\cdot}nH_2O$
4127 (13,541)	4	$K_{0.5}(Al_{1.7}Fe_{0.3}Mg_{0.1})(Si_{3.6}Al_{0.4})O_{10}(OH)_2{\cdot}nH_2O$
	5	$K_{0.3}Ca_{0.03}(Al_{1.6}Fe_{0.3}Mg_{0.2})(Si_{3.6}Al_{0.4})O_{10}(OH)_2{\cdot}nH_2O$

https://doi.org/10.1346/CCMN.1997.0450112 Published online by Cambridge University Press

Figure 6. TEM image of sample from 4127 m. The arrow indicates an illite packet analyzed by EDS. The clay composition of this area is indicated by stoichiometry #4 in Table 1. A second analysis was taken that included both the packet and its surrounding, less illitic, matrix and is given by stoichiometry #5 in Table 1.

illite may correspond to detrital illite in mudrocks above the zone of illitization. However, within the transition zone and deeper, the measurement of discrete illite includes both original detrital illite and larger packets of authigenic illite.

Especially interesting clay textures related to the illitization reaction were captured in a TEM image taken from the shallowest, most smectitic sample examined by TEM (2899 m). In this image, a packet of discrete illite, probably of detrital origin, is surrounded by smectite (Figure 7). Note that a few clay layers extend continuously from the illite into the smectite. This image may be showing an area where an illite packet has grown at the expense of smectite layers. The thin area between the end of the illite packet and the smectite layers (indicated by an arrow in Figure 8) is mostly disordered, which can be taken as evidence of dissolution/reprecipitation of 2:1 layers during illitization.

Alternatively, the image in Figure 7 could be evidence of a frozen retrograde reaction of illite to smectite. According to Velde and Vasseur (1992), this retrograde reaction occurs at shallow depths in sedimentary sequences. The TEM study of Jiang et al. (1990) noted replacement of illite by mixed-layer illite/smectite in mudrocks from an Ordovician prograde metamorphic sequence.

Mineralogical Changes Coincident with Illitization

Formation of Fe-rich chlorite has been postulated to be a potential sink for Fe generated by illitization. In TEM images of mudrocks, we occasionally observed Fe-rich chlorite layers, identified as chlorite by the characteristic 14-Å interlayer spacings (Spinnler et al. 1984). A detrital grain of chlorite was identified in TEM images in the sample from 2899 m (Figure 8a). Chlorite that we interpret as authigenic was imaged in the sample from 3829 m (Figure 8b). This chlorite consists of 4 layers in the midst of 10-Å illite and smectite. Three of these layers have the standard 14-Å chlorite spacing, while the other has a 21-Å interlayer spacing. A 21-Å spacing in chlorite may arise from a planar defect, such as a missing layer, that interrupts the regular alternation of brucite and talc layers within the chlorite structure (Veblen 1983). An authigenic origin for this chlorite is proposed because it is so thin and intimately intermixed with mixed-layer clay. Similar occurrences of authigenic chlorite were reported by Ahn and Peacor (1985).

Development of quartz overgrowths in diagenetically altered rocks has been attributed to Si generated during the smectite-to-illite reaction. During the course of our TEM work, we found no evidence of such authigenic quartz.

DISCUSSION

Solid-State Reaction versus Dissolution/Reprecipitation

Two reaction mechanisms may be invoked to describe illitization of smectite: 1) solid-state reactions, and 2) dissolution-precipitation reactions (Bethke and Altaner 1986). In the solid-state mechanism, the 2:1 layers of smectite maintain their integrity throughout the reaction (Hower et al. 1976). In this model, the reaction occurs by ionic substitution of Al for Si within intact tetrahedral sheets. Potassium then replaces all other exchangeable cations in the interlayer sites. K-feldspar dissolution is considered to be the source of Al and K required for the reaction. Boles and Franks (1979) write the equation for this "layer-conserving" reaction as follows:

$$KNaCa_{22}Mg_4Fe_4Al_{14}Si_{38}O_{100}(OH)_{20} + 10H_2O + 4.5K + 8Al \rightarrow K_{5.5}Mg_2Fe_{1.5}Al_{22}Si_{35}O_{100}(OH)_{20} + Na + 2Ca + 2.5Fe + 2Mg + 3Si + 10H_2O \quad [3]$$

An important feature of the above reaction is that 1 mole of smectite reacts to 1 mole of illite; on a molar basis, no clay is gained or lost.

Alternatively, the dissolution-precipitation mechanism entails dissolution of existing 2:1 layers in smectite, followed by formation of new illite layers. An important aspect of this mechanism is that an external source of Al is not necessary, even though illite has proportionally more Al than smectite. In this model, reprecipitation of illite is limited by the amount of Al available from smectite dissolution. Without an external source of Al, dissolution of smectite layers results in reprecipitation of fewer illite layers. Boles and Franks (1979) wrote a reaction consistent with the dissolution-precipitation mechanism as follows:

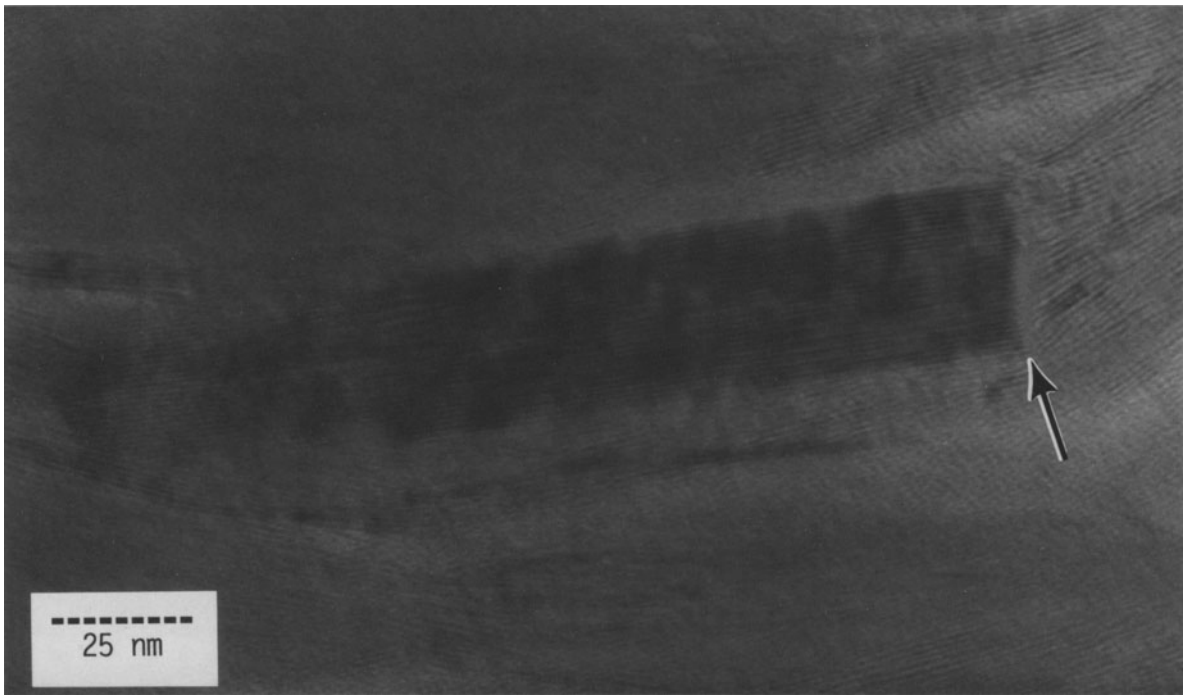

Figure 7. TEM image of sample from 2899 m. A packet of discrete detrital illite is prominent in the center of the image and is surrounded by smectite. The strictly parallel 10-Å clay layers within the packet are characteristic of illite. At the interface between illite and smectite marked by the arrow, some clay layers appear to be continuous from the illite into the smectite.

$$1.57KNaCa_2Mg_4Fe_4Al_{14}Si_{38}O_{100}(OH)_{20} + 10H_2O + 3.93K \rightarrow K_{5.5}Mg_2Fe_{1.5}Al_{22}Si_{35}O_{100}(OH)_{20} + 1.57Na + 3.14Ca + 4.28Mg + 4.78Fe + 24.66Si + 57O + 11.4(OH) + 15.7H_2O \quad [4]$$

Comparing the "layer-conserving" and the "Al-conserving" reactions on a molar basis shows that, per unit of smectite consumed, the latter mechanism generates 36% less illite (Boles and Franks 1979). The "Al-conserving" reaction also releases 5.1 times more Si, 1.2 times more Fe and 1.4 times more Mg than the "layer-conserving" reaction. In addition, the "Al-conserving" reaction requires 56% less K than the "layer-conserving" reaction.

If the original detrital content of illite and smectite in mudrocks from the study well was relatively constant, a decrease in total illite and smectite coincident with the smectite-to-illite reaction would be supporting evidence for the "Al-conserving" reaction and the dissolution-reprecipitation mechanism. A decrease with depth in the total amount of illite and mixed-layer illite/smectite clay is evident in the data of Hower et al. (1976), and was considered by Boles and Franks (1979) as support for the "Al-conserving" reaction. The XRD data collected in this study shows that the increase in total illite (discrete illite plus mixed-layer illite) is less than the observed decrease in smectite (Figure 9). Therefore, our XRD data also indicate a net loss in illite/smectite, and support the "Al-conserving" reaction.

TEM images of I/S clay also support the dissolution-reprecipitation and "Al-conserving" reaction mechanism. Illitization in these images is not more pronounced at the edges of clay masses. Illitization appears to occur as readily within clay-rich areas as at the more exposed fringe areas of clay masses (Figure 6). We interpret these textures as further evidence supporting illitization of smectite without the need to invoke an external source of Al. While migration of ions at this scale in clays may readily occur, it seems unlikely that components from an external source (Al or K) would preferentially react with internal, isolated smectite rather than with smectite at the edges of clay masses.

Role of K in Illitization

A study of cuttings from the GOM COST 1 well suggests that illitization is a 2-step process (Bell 1986). The first step is creation of high-charge, Al-enriched layers by either of the mechanisms described above. The second step, which may occur much later, is fixation of K and dehydration. Bell (1986) observed that saturation of smectite-rich samples by K caused significant decreases in the amounts of expandable clay in cuttings from shallower depths (to 760 m),

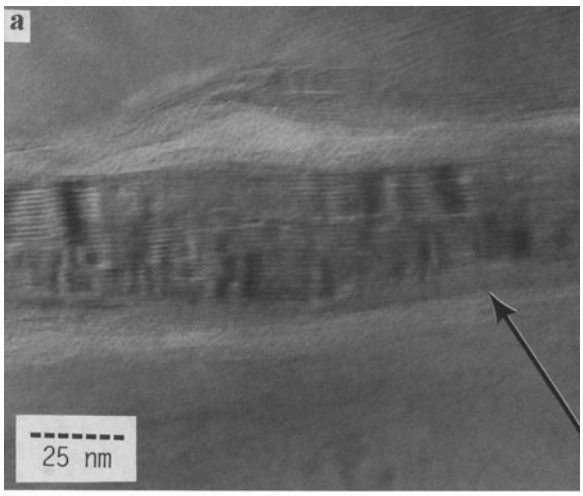

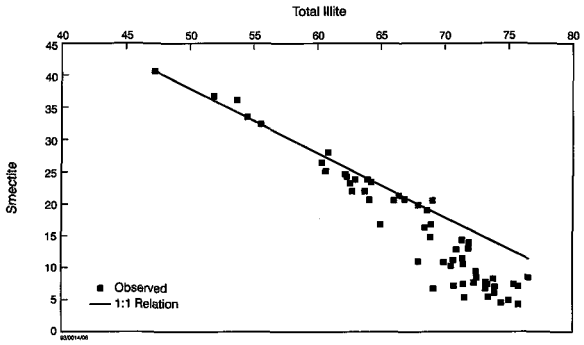

Figure 9. Plot of XRD data from 60 mudrock samples in the study well. This plot of total smectite (wt% smectite; mixed-layer clay) vs. total illite (wt% illite; mixed-layer clay + discrete illite). The data deviate from the line representing 1-to-1 replacement of smectite by illite. We interpret these data as evidence in support of an illitization reaction in which clay layers are not conserved.

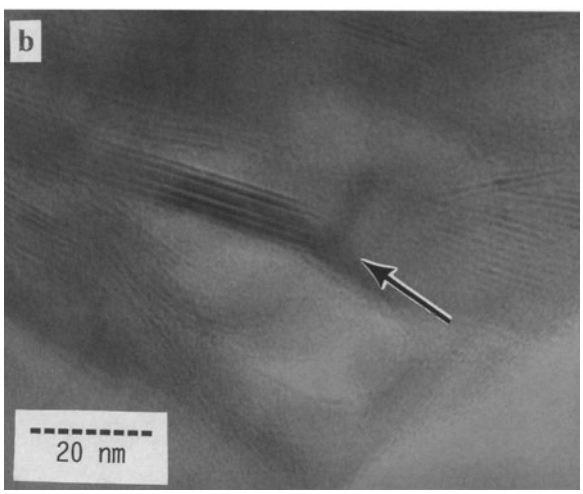

Figure 8. TEM images of chlorite. a) TEM image of sample from 2899 m. The clay flake indicated by the arrow is chlorite. It is identified by its 14-Å interlayer spacings and by its Fe-rich EDS spectrum. b) TEM image of sample from 3829 m. The arrow points to a 4-layer-thick crystallite of chlorite interpreted to be of authigenic origin.

while the effect of saturation by K on deeper samples was less pronounced. He concluded that high-charge, Al-rich layers formed at shallower depths, but lack of available K prevented complete conversion of this material to true illite. In the GOM COST 1 well, K-feldspar dissolves to supply K at about 760 m (~2500 ft). Below this significant K-feldspar dissolution, nearly all high-charged layers are completely illitized.

Some of our TEM and EDS observations support a 2-step mechanism for illitization of smectite, in which creation of high-charge smectite is followed by incorporation of K. An EDS spectrum collected from a spot on an illite packet (Figure 6) produced an illitic stoichiometry. Another EDS spectrum was taken that included mostly mixed-layer clay surrounding the illite packet. The Al/Si ratio estimated from this second spectrum is the same as that estimated from the first, illite-only spectrum. However, the second spectrum showed that the mixed-layer clay contains substantially less K (compare stoichiometries 4 and 5 in Table 1). The illitic Al/Si ratio of the clay surrounding the illite packet suggests that it has undergone Al-for-Si substitution and has an increased layer charge. However, the lower concentration of K in this clay indicates that K fixation has not yet converted all of this clay to illite. Our XRD data show little evidence of correlation between K-feldspar dissolution and illitization.

Effects of Illitization on Mudrock Porosity and Permeability

The effects of the smectite-to-illite transition on porosity and permeability in mudrocks are poorly understood. Based on the observations that illite has a more ordered structure than smectite, and that disordered smectite should favor movement of fluids, Freed and Peacor (1989b) suggested that illitization should reduce permeability. In contrast, the work of Howard (1991) indicates that illite-rich shales are more permeable than adjacent, more smectitic shales.

Our TEM images show that in non-illitized mudrocks there is a continuous matrix of smectitic mixed-layer clay that appears to effectively fill all space between grains. The clay matrix of more illitized mudrocks appears less continuous, with well-defined, slightly separated thin crystallites of illite. Such images suggest that illitization may increase mudrock permeability. Textural interpretation of these TEM images is speculative because of the possibility that critical textures have been influenced by sample collection (sidewall coring) or by sample preparation (ion-milling). A decrease in clay volume accompanying the

https://doi.org/10.1346/CCMN.1997.0450112 Published online by Cambridge University Press

smectite-to-illite reaction, part of the "Al-conserving" reaction model of Boles and Frank (1979), would also seem to favor increased porosity and permeability. Loss of clay volume may lead to increased porosity particularly in geopressured zones, where compaction would be retarded by anomalously high fluid pressures. Finally, the wireline log responses commonly associated with geopressured zones—decreased density, velocity and resistivity—all are indicative of greater mudrock porosity.

CONCLUSIONS

Previous studies of the smectite- to-illite reaction in GOM sediments have concentrated on Miocene-age mudrocks. Here we have documented this reaction in younger Pliocene-age sediments collected as sidewall cores from a GOM continental shelf well.

TEM imaging of selected mudrock samples shows that packets of discrete illite are more prevalent and larger in samples from greater depths and higher temperatures. XRD analysis confirms that the discrete illite component increases with depth, and shows that the proportion of illite in mixed-layer clay also increases. These observations suggest 2 modes of illitization: 1) overgrowth of authigenic illite on discrete illite packets, and 2) creation of new illite layers within the mixed-layer clay component. Detrital and authigenic chlorite packets were detected in TEM images of mudrocks from the study well. The authigenic chlorite is a likely sink for Fe and Mg evolved from the smectite-to-illite reaction.

Our TEM and XRD observations support the "Al-conserving" mechanism for the illitization of smectite as proposed by Boles and Franks (1979). This mechanism allows the reaction to occur without an external source of Al. Our results do not lead to definitive conclusions regarding the role of K in illitization of these samples. XRD analyses of our samples show little correlation between dissolution of K-bearing feldspar and illitization. In one sample, our TEM/EDS study detected high-charge smectite, indicative of conditions in which there is insufficient K for illite formation.

ACKNOWLEDGMENTS

We would like to thank our colleagues T. Taylor and T. Diggs for critical review and discussion of this paper. We also thank the management of Shell Oil Company for permission to publish this work.

REFERENCES

Ahn JH, Buseck PR. 1990. Layer-stacking sequences and structural disorder in mixed-layer illite/smectite: Image simulation and TEM imaging. Am Mineral 75:267–275.

Ahn JH, Peacor DR. 1985. Transmission electron microscopic study of diagenetic chlorite in Gulf Coast argillaceous sediments. Clays Clay Miner 33:228–236.

Ahn JH, Peacor DR. 1986. Transmission and analytical electron microscopy of the smectite to illite transition. Clays Clay Miner 34:165–179.

Bell TE. 1986. Microstructure in mixed-layer illite/smectite and its relationship to the reaction of smectite to illite. Clays Clay Miner 34:146–154.

Bethke CM, Altaner SP. 1986. Layer-by-layer mechanism of smectite illitization and application to a new rate law. Clays Clay Miner 34:136–145.

Boles JR, Franks SG. 1979. Clay diagenesis in the Wilcox sandstones of Southwest Texas: Implications of smectite diagenesis on sandstone cementation. J Sed Petrol 49:55–70.

Burst JF. 1969. Diagenesis of Gulf Coast clayey sediments and its possible relation to petroleum migration. Bull Am Assoc Petrol Geol 53:73–93.

Eberl D. 1993. Three zones for illite formation during burial diagenesis and metamorphism. Clays Clay Miner 41:26–37.

Freed RL, Peacor DR. 1989a. Variability in the temperature of the smectite/illite reaction in Gulf Coast sediments. Clay Miner 24:171–180.

Freed RL, Peacor DR. 1989b. Geopressured shale and sealing effect of smectite to illite transition. AAPG Bull 73: 1223–1232.

Guthrie GD Jr, Veblen DR. 1989. High-resolution transmission electron microscopy of mixed-layer illite/smectite: Computer simulations. Clays Clay Miner 37:1–11.

Howard JJ. 1991. Porosimetry measurement of shale fabric and its relationship to illite/smectite diagenesis. Clays Clay Miner 39:355–361.

Hower J. 1981. Shale diagenesis. In: Longstaffe FT, editor. Clays and the resource geologist. Short course handbook 7. Ottawa: Mineral Assoc Canada. p 60–80.

Hower J, Eslinger EV, Hower M, Perry EA. 1976. Mechanism of burial metamorphism of argillaceous sediment: 1. Mineralogical and chemical evidence. GSA Bull 87:725–737.

Jiang WT, Peacor DR, Merriman RJ, Roberts B. 1990. Transmission and analytical electron microscopic study of mixed-layer illite/smectite formed as an apparent replacement product of diagenetic illite. Clays Clay Miner 38: 449–468.

Klimentides RE, MacKinnon IDR. 1986. High-resolution imaging of ordered mixed-layer clays. Clays Clay Miner 34:155–164.

MacKinnon IDR. 1990. Low-temperature analyses in the analytical electron microscope. In: MacKinnon IDR, Mumpton FA, editors. CMS workshop lectures, vol. 2: Electron-optical methods in clay science. Boulder, CO: Clay Miner Soc. p 90–106.

Moore DM, Reynolds RC. 1989. X-ray diffraction and the identification and analysis of clay minerals. NY: Oxford Univ Pr. 384 p.

Pearson MJ, Watkins D, Small JS. 1982. Clay diagenesis and organic maturation in Northern North Sea sediments. Proc Int Clay Conf; Italy. p 665–675.

Perry E, Hower J. 1970. Burial diagenesis in Gulf Coast pelitic sediments. Clays Clay Miner 18:165–177.

Shaw HF, Primmer TJ. 1989. Diagenesis in shales from a partly overpressured sequence in the Gulf Coast, Texas, USA. Marine Petrol Geol 6:121–128.

Spinnler GE, Self PG, Iijima S, Buseck PR. 1984. Stacking disorder in clinochlore chlorite. Am Mineral 69:252–263.

Surdam RC, Crossey LJ. 1987. Integrated diagenetic modeling: A process-oriented approach for clastic systems. Annu Rev Earth Planet Sci 15:141–170.

Vali H, Koster HM. 1986. Expanding behavior, structural disorder, regular and random irregular interstratification of 2:1 layer silicates studied by high-resolution images of transmission electron microscopy. Clay Miner 21:827–859.

Veblen DR. 1983. Microstructures and mixed layering in intergrown wonesite, chlorite, talc, biotite, and kaolinite. Am Mineral 68:566–580.

Veblen DR, Guthrie GD Jr, Livi KJT, Reynolds RC Jr. 1990. High-resolution transmission electron microscopy and electron diffraction of mixed-layer illite/smectite: Experimental results. Clays Clay Miner 38:1–13.

Velde B, Vasseur G. 1992. Estimation of the diagenetic smectite to illite transformation in time-temperature space. Am Mineral 77:967–976.

(Received 15 February 1995; accepted 25 April 1996; Ms. 2620)